Fuel 417 (2026) 138537

Contents lists available at ScienceDirect

Fuel

journal homepage: www.elsevier.com/locate/jfue

Full length article

Urea decomposition, oxidation, and SNCR: The effect of CO

Claudia Pastor-Morell [a], Hamid Hashemi [a], Hao Wu [a], Peter Glarborg [a,*], Alberto Cuoci [b]

[a] DTU Chemical Engineering, Technical University of Denmark, DK-2800 Lyngby, Denmark
[b] CRECK Modeling Lab, Department of Chemistry, Materials, and Chemical Engineering, Politecnico di Milano, 20133 Milan, Italy

HIGHLIGHTS

- Urea decomposition, oxidation, and SNCR process are investigated in a flow reactor at 973–1473 K.
- An updated detailed reaction mechanism is validated against present and previous experimental data.
- Urea oxidation and SNCR chemistry are strongly promoted in the presence of CO.
- High temperature and high CO cause breakdown of PFR approximation due to radial temperature gradients in preheating zone.
- Multidimensional modeling offers an accurate description of the conversion in fast reacting zones under high CO loading.

ARTICLE INFO

Keywords:
Urea decomposition
Urea oxidation
SNCR
Flow reactor
PFR assumption

ABSTRACT

Urea decomposition and oxidation at high temperatures, along with its interaction with NO in the SNCR process, have been investigated through a combination of flow reactor experiments and detailed chemical kinetic modeling. The experiments were performed at atmospheric pressure using $CO(NH_2)_2/H_2O$ mixtures, investigating the effect of adding O_2, NO, and/or CO. The experiments were highly diluted in N_2 and the temperature was varied from 973 to 1473 K. The reaction mechanism was based on the nitrogen chemistry review by Glarborg et al. (2018), with updates to the amine, HNCO, and N_2O subsets based on more recent studies. Thermal urea decomposition and oxidation experiments were consistent with the theoretical rate constant for gas-phase urea dissociation proposed by Honorien et al. (2021), which deviates significantly from previously used values in SNCR modeling with urea. Adding CO has a similar effect on both urea oxidation and SNCR, shifting the chemistry towards lower temperatures. In the SNCR process, the temperature for maximum NO removal shifted by up to 200 K without compromising the overall reduction efficiency. A breakdown of the plug-flow approximation was observed at elevated temperatures and high CO concentrations, attributed to reactions occurring in the preheating zone, where strong radial temperature gradients are present. Under these conditions, cylindrical shear flow reactor models and full two-dimensional simulations provided more accurate predictions. Overall, the modeling predictions were in good agreement with both the experimental data from this study and literature data.

1. Introduction

In 2019, the European Commission listed Selective Catalytic Reduction (SCR) and Selective Non-Catalytic Reduction (SNCR) technologies as Best Available Techniques (BAT) to mitigate nitrogen oxides (NO_x) emissions during combustion in Waste to Energy (WtE) plants [1]. SNCR is often chosen over alternative methods for its simplicity, lack of catalyst, and ease of installation in existing plants [2–5]. The process involves injecting a reducing agent into the flue gas that reacts with NO_x to produce primarily N_2 and H_2O. The reaction occurs within a temperature window of 1123–1423 K [2,6–8], depending on the choice of reducing agent, the composition of the flue gas, and the mixing in the furnace.

In most full-scale applications, either ammonia or aqueous urea is used as the reducing agent. The urea-based SNCR process was first proposed by Muzio and coworkers [9] and is commonly referred to as the NO_xOut process. At high temperatures, urea decomposes rapidly to NH_3 and HNCO, resulting in a chemistry that is closely related to both Thermal DeNO_x (SNCR with ammonia) and RapReNO_x (SNCR with cyanuric acid) [10]. The injection of aqueous urea instead of ammonia is of interest because it offers a safer and more convenient option for storage, handling, and transportation [11,12]. However, the main drawback of

* Corresponding author.
Email address: pgl@kt.dtu.dk (P. Glarborg).

https://doi.org/10.1016/j.fuel.2026.138537
Received 10 September 2025; Received in revised form 3 December 2025; Accepted 24 January 2026
Available online 7 February 2026

the process is that, similarly to RapReNO$_x$, the strong greenhouse gas N_2O will be formed and may be emitted from the process.

The efficiency of the SNCR process is affected by fluctuations in flue gas composition. Jepsen [13] reported fluctuations in CO concentration in the first pass of a full-scale WtE furnace, mostly between 0 and 2000 ppm, with peaks up to 7000 ppm. Several studies have shown that CO affects SNCR by shifting the effective temperature window for NO reduction to lower temperatures [6,14–18]. However, most of these studies focus on ammonia-based SNCR and less is known about the impact of CO on urea-based SNCR.

Despite its commercial relevance, the NO$_x$Out process remains less well characterized than Thermal DeNO$_x$. Experimental data for the NO$_x$Out process under well-defined laboratory conditions are limited [10]. In laboratory scale, tubular flow reactor experiments results have been reported by Alzueta et al. [16], Lee et al. [19], and Wang et al. [12], while Rota et al. [20,21] performed experiments in a jet-stirred reactor. Chemical kinetic models for the NO$_x$Out process have been reported by several groups [20–22]. The reaction mechanism involves reactions for urea decomposition, along with the H/N/O subset for Thermal DeNO$_x$ and the HNCO subset for RapReNO$_x$. However, the kinetic models developed involve uncertainties related to the behavior of urea at high temperatures and high heating rates [10,22]. The available experimental data are not fully consistent and the accuracy of reported kinetic mechanisms is uncertain.

In a urea-water droplet, the decomposition can occur directly in the condensed phase, or it can involve evaporation followed by decomposition in the gas-phase. The decomposition behavior has implications for both the reaction rates and the resulting products. In recent years, gas-phase decomposition has been the primary focus, particularly under SCR conditions [23–26]. However, validation at high temperature conditions is scarce.

The present work aims to improve the understanding of urea decomposition and oxidation at high temperatures, as well as its interaction with NO in the NO$_x$Out process. Atmospheric pressure tubular flow reactor experiments are conducted with a CO(NH$_2$)$_2$/H$_2$O mixture, highly diluted in N_2, investigating the effect of adding various amounts of O_2, NO, and/or CO. The temperature is varied in the range of 973–1473 K and the effect of adding CO is investigated. A chemical kinetic model, based on previous work by the authors [10,27,28], is developed for the gas-phase decomposition and oxidation of urea and verified against the present experimental data, as well as results from literature.

This work also addresses the modeling limitations that arise for tubular flow reactors when fast chemistry occurs under strong thermal gradients, induced here by high CO concentrations. This scenario is examined through detailed simulations using a 2D axisymmetric reactor model, a set of 1D models including Taylor-Aris dispersion corrections, a plug-flow reactor model, and a cylindrical shear flow reactor model.

2. Experimental setup and procedure

The experimental setup included a gas feeding panel, an atomizer, a quartz reactor placed in an electrically heated oven, and a Fourier Transform Infrared (FTIR) spectrometer for downstream analysis. A schematic overview of the setup is shown in Fig. 1.

The reactor consisted of a quartz tube with an internal diameter of 6 mm. It was placed in a 60 cm long electrically heated 3-zone oven. High-purity gases (AGA, Air Liquide) were supplied from gas cylinders, controlled by separate mass flow controllers. An atomizer was used to dose the urea-water solution. The atomizer produced aerosols with an average droplet size in the range of 0.02–0.3 μm [29]. The solution was prepared using urea pellets (>99.5 % Sigma-Aldrich Corp.) and deionized water. The carrier gas was passed through an orifice in the atomizer body. The aerosols produced were transported through a 12 mm i.d. tube, designed to minimize the impact of condensation, to a mixing zone, where they were mixed with the remaining gases before entering the heated part of the reactor. In all experiments, the total gas flow rate was maintained at 2.0 L/min (298 K, 1 atm). For CO dosing, an activated carbon filter was added upstream of the mass flow controller to remove iron carbonyls which might have been generated by CO reaction with the iron in the gas bottle.

In the oven, the gas mixture was rapidly heated to the desired set temperature. The temperature of the reactor was monitored using a type K thermocouple placed at the top of the furnace while a nitrogen flow was maintained to obtain axial temperature profiles as shown in Fig. 2. The results showed an isothermal region of 40 cm, beyond which the product gas was rapidly cooled. The uncertainty in the isothermal temperature (± 10 K), accounts for both measurement accuracy (± 2 K) and deviations from the mean. The temperature increase from chemical reaction was at most 13 K (adiabatic, with 1000 ppm CO), but in reality it was less due to heat transfer to the walls and surroundings.

The product gas was kept at 453 K to avoid condensation of water prior to analysis. The gas composition was measured using an FTIR analyzer (Gasmet DX4015) at 453 K. The concentrations of HNCO, CO, CO_2, H_2O, NO, N_2O, NO_2, and NH_3 were determined, with measuring ranges set to 0–1000 ppm for HNCO, 0–2 % for CO, 0–2 % for CO_2, 0–16 % for H_2O, 0–2000 ppm for NO, 0–500 ppm for N_2O, 0–500 ppm for NO_2, and 0–5000 ppm for NH_3. Disregarding cross-interference, the uncertainty

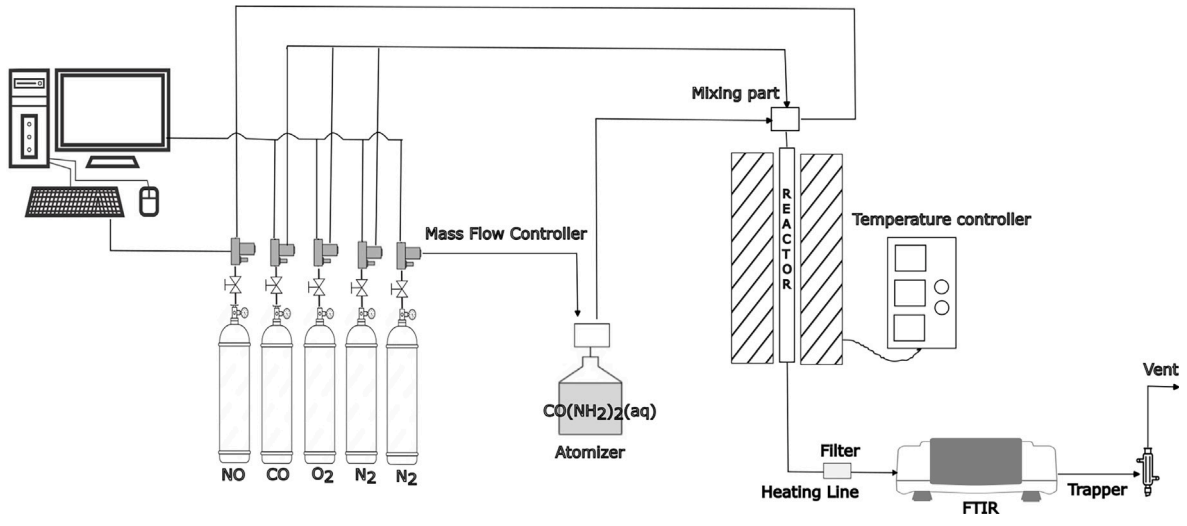

Fig. 1. Schematic of the flow reactor setup.

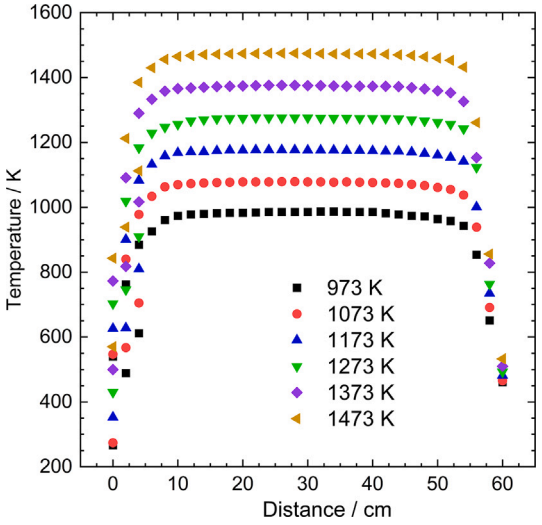

Fig. 2. Selected axial temperature profiles in the reactor. The temperatures were measured with a type K thermocouple from the top of the oven under a nitrogen flow.

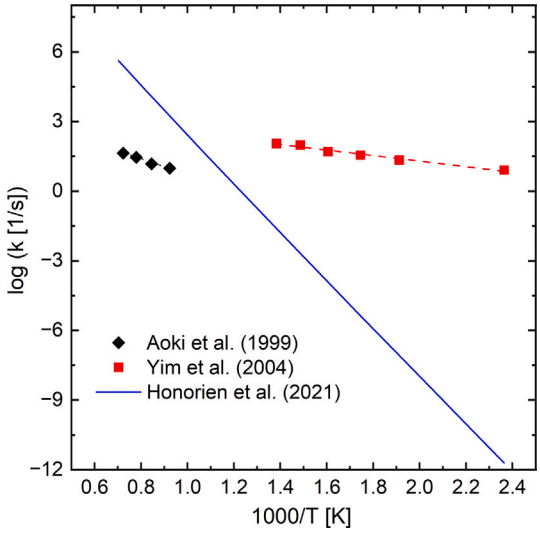

Fig. 3. Arrhenius plot for reaction 1. The symbols denote experimental measurements, the dashed lines denote calculated values, and the solid line denotes a theoretical determination. Data were drawn from the following sources: Aoki et al. [53], Yim et al. [54], and Honorien et al. [32].

of these measurements is estimated to be within 2 % of the measuring ranges. The initial urea concentration was determined from a carbon balance under oxidizing conditions at high temperature, where HNCO and CO were largely oxidized to CO_2. The carbon balance, as well as the water content for each experiment, is provided in the Supplementary Material.

3. Detailed chemical kinetic model

The chemical kinetic model adopted in this work, including rate coefficients and thermodynamic data, is based on the nitrogen chemistry review by Glarborg et al. [10], with modifications drawn from more recent studies. The H_2-O_2 and amine subsets were updated according to Jian et al. [27], while the HNCO and N_2O subsets were drawn from Morell et al. [28] and Glarborg and coworkers [30,31], respectively. Table 1 lists selected reactions from the $CO(NH_2)_2$, NH_3, and HNCO subsets, and the full mechanism is available as Supplementary Material.

Table 1
Selected reactions for $CO(NH_2)_2$, NH_3, and HNCO subsets. Reaction rate parameters are given for the modified Arrhenius expression: $k = AT^{\beta}\exp(-E_a/[RT])$. Units are mol, cm, s, cal. The full mechanism is available in the Supplementary Material.

		A	β	E_a	Source
1.	$CO(NH_2)_2 \rightleftarrows NH_3 + HNCO$	6.9E06	1.810	45,311	[32]
2.	$HNCO + H_2O \rightleftarrows NH_3 + CO_2$	2.0E13	0.000	48,500	[10]
3.	$HNCO + M \rightleftarrows NH + CO + M$	1.1E16	0.000	86,000	[33]
4.	$HNCO + OH \rightleftarrows NCO + H_2O$	3.5E07	1.500	3600	[34]
5.	$NCO + O \rightleftarrows NO + CO$	2.0E15	−0.500	0	[35]
6.	$NCO + O_2 \rightleftarrows NO + CO_2$	2.0E12	0.000	20,000	[36] est
7.	$NCO + NO \rightleftarrows N_2O + CO$	4.0E19	−2.190	1743	[37]
8.	$NCO + NO \rightleftarrows N_2 + CO_2$	1.5E21	−2.740	1824	[37]
9.	$NH_3 + OH \rightleftarrows NH_2 + H_2O$	2.0E06	2.040	566	[38]
10.	$NH_2 + O \rightleftarrows HNO + H$	2.8E13	−0.065	−188	[39]
11.	$NH_2 + OH \rightleftarrows NH + H_2O$	3.3E06	1.949	−217	[40,41]
12.	$NH_2 + O_2 \rightleftarrows H_2NO + O$	2.6E11	0.487	29,050	[41]
13.	$NH_2 + NO \rightleftarrows N_2 + H_2O$	2.6E19	−2.369	870	[42]
14.	$NH_2 + NO \rightleftarrows NNH + OH$	4.3E10	0.294	−866	[42]
15.	$NH + O_2 \rightleftarrows NO + OH$	4.5E08	0.790	1200	[43]
16.	$NH + O_2 \rightleftarrows HNO + O$	2.1E13	0.000	15,800	[43]
17.	$NO + HO_2 \rightleftarrows NO_2 + OH$	2.1E12	0.000	−497	[44]
18.	$CO + OH \rightleftarrows CO_2 + H$	8.7E05	1.730	−685	[45]
19.	$OH + OH \rightleftarrows O + H_2O$	2.0E07	1.651	631	[10]
		2.6E11	−0.057	−827	[10]
20.	$H + O_2 \rightleftarrows O + OH$	1.0E14	0.000	15,286	[46]
21.	$H + O_2(+M) \rightleftarrows HO_2(+M)$	1.2E12	0.580	−214	[47]
	Low pressure limit	4.6E20	−1.670	871	[47]
22.	$HO_2 + OH \rightleftarrows H_2O + O_2$	1.9E20	−2.490	584	[48]
		1.2E09	1.240	−1310	[48]

At temperatures above 600 K, the generally accepted pathway for the thermal decomposition of urea involves the formation of ammonia and isocyanic acid (R1) [15,16,49–52],

$$CO(NH_2)_2 \rightarrow NH_3 + HNCO \quad \text{(R1)}$$

Under high-temperature and rapid-heating conditions, urea decomposition is often assumed to occur instantaneously [16,51]. However, the gas-phase kinetics of urea decomposition have been investigated both experimentally [53,54] and theoretically [32]. Fig. 3 shows an Arrhenius plot for R1. Aoki et al. [53] and Yim et al. [54] derived values of k_1 from flow reactor experiments in a ceramic tube reactor (1083-1383 K) and an alumina reactor filled with glass beads (423-723 K), respectively. Honorien et al. [32] calculated a rate constant for R1 from electronic structure calculations and transition state theory.

The theoretical study by Honorien et al. [32] indicates a large barrier for gas-phase urea dissociation. The low activation energies for R1 reported in the experimental studies are unlikely to represent true gas-phase dissociation, and may instead reflect contributions from condensed-phase reactions or reactions on alumina/glass surfaces. Consequently, we adopt the theoretical rate constant proposed by Honorien et al. It has been proposed that urea decomposition may yield radicals directly, either as $NH_2 + H_2NCO$ [55] or $NH_2 + H + HNCO$ [56], but both of these steps are strongly endothermic and would be too slow to play a role in the process.

In the presence of water, it has been suggested that urea decomposes through thermohydrolysis, $CO(NH_2)_2 + H_2O \rightarrow 2NH_3 + CO_2$ [51,53]. This step could occur directly or through the sequence of reaction R1 and the isocyanic acid hydrolysis reaction,

$$HNCO + H_2O \rightarrow NH_3 + CO_2 \quad \text{(R2)}$$

Experimental rate data for reaction R2 are currently unavailable. Following Glarborg et al. [10], this reaction is included with an estimated pre-exponential factor of 2×10^{13} cm^3 mol^{-1} s^{-1} and an activation energy of 48.5 kcal mol^{-1}. Inclusion of $CO(NH_2)_2 + H_2O$ with a similar rate constant has no effect on modeling predictions.

4. Results and discussion

Flow reactor experiments were performed at atmospheric pressure in the temperature range of 973–1473 K using $CO(NH_2)_2/H_2O$ mixtures with varying amounts of O_2, NO, and CO, and highly diluted in N_2. A listing of the experimental conditions is shown in Table 2. The maximum uncertainty in the initial $CO(NH_2)_2$ and H_2O concentrations over the investigated temperature range was ±28 ppm and ±0.3 % (1σ), respectively.

To address potential modeling limitations, several modeling approaches were tested. These included a conventional plug-flow reactor (PFR); a cylindrical shear-flow reactor (CSFR) accounting for radial diffusion; a one-dimensional (1D) model with axial diffusion and conduction, tested with and without the Taylor-Aris correction for heat and mass transport; and a two-dimensional (2D) axisymmetric reactor including back diffusion. Most simulations were performed using Chemkin-Pro, part of the ANSYS Fluent software package [57]. However 1D simulations were conducted with the OpenSMOKE++ Suite, while two-dimensional 2D simulations were performed using laminarSMOKE++ [58,59]. Unless otherwise specified, simulations were conducted for ideal plug flow, incorporating the full measured temperature profile to account for the preheating, isothermal, and outlet zones of the reactor. Additional information on the modeling approaches is provided in the Supplementary Material.

4.1. Thermal decomposition of $CO(NH_2)_2$

Fig. 4 shows the products formed during the thermal decomposition of aqueous urea aerosols. Above 973 K, urea predominantly decomposed into NH_3 and HNCO, which remained stable across the studied temperature range. Above 1373 K, NH_3 slightly increased, HNCO decreased, and small traces of CO and CO_2 were detected, likely due to HNCO hydrolysis (R2) and thermal decomposition (R3). The modeling predictions align well with the experimental results, supporting the proposed gas-phase reaction pathway $CO(NH_2)_2 = NH_3 + HNCO$. Simulations along the reactor at different temperatures show that urea decomposes rapidly in the preheating zone at temperatures above 1023 K (see the Supplementary Material). Presumably close to the high-pressure limit, the dissociation rate of urea is not expected to depend on the bath gas composition. Direct reaction with other gas-phase components is unlikely to be competitive. The molar ratio of NH_3 to HNCO was approximately 1.0, increasing to 1.1 with rising temperature. Aoki et al. [53] reported ratios ranging from 1 to 1.5, depending on the temperature and residence time in the reactor, with higher ratios observed at elevated temperatures or longer residence times. Chen et al. [60] reported values between 1.2 and 1.7 over a temperature range of 800 to 1273 K. The lower ratios observed in the present work are attributed to shorter residence times, which reduce the extent of secondary reactions.

Table 2
Experimental conditions. The balance gas is N_2, and the total flow rate is 2000 mL min^{-1} (298 K, 1 atm). Species concentrations are given in ppm or % (O_2, H_2O).

Set	$CO(NH_2)_2$	CO	NO	NO_2	O_2	H_2O
1	252	0	0	0	0	3.5
2	255	0	0	0	5	3.3
3	250	0	0	0	97.4	2.6
4	245	244	0	0	5	3.4
5	250	1020	0	0	5	3.4
6	305	0	200	11	5	3.6
7	300	248	181	28	5	3.2
8	312	1011	187	30	5	3.3
9-R1	341	200–1000*	194	22	5	3.2
9-R2	299	200–1000*	184	25	5	3.1

*CO concentrations of 200, 400, 600, 800 and 1000 ppm.

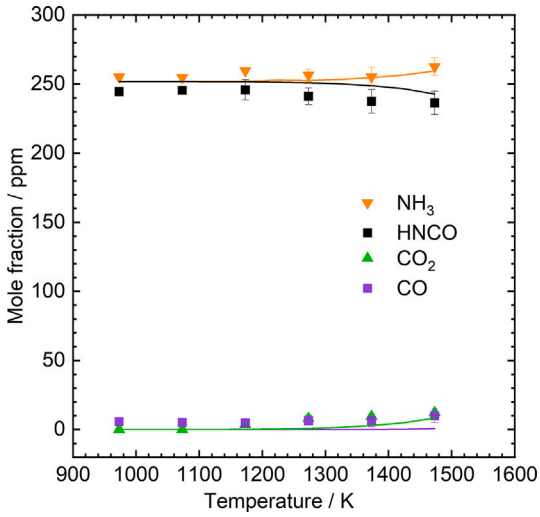

Fig. 4. Urea decomposition as a function of temperature. Symbols represent experimental data, while solid lines denote predictions from the PFR model. Error bars indicate the standard deviation from replicate experiments. Inlet conditions: $CO(NH_2)_2$ = 252 ppm, H_2O = 3.5 % and N_2 balance. P = 1.05 atm. The residence time in the isothermal zone was 101/T[K] s (constant mass flow).

4.2. Oxidation of $CO(NH_2)_2$

The oxidation of urea was investigated at oxygen concentrations of 5 % and 97 %, as shown in Fig. 5. At 5 % of O_2, NH_3 and HNCO started to be consumed at 1273 K, entering a rapid oxidation regime at higher temperatures. Above this temperature NO, N_2O, CO, and CO_2 were produced, with CO_2 being the major product. Under 97 % O_2, the onset temperatures for NH_3 and HNCO oxidation decreased to 1073 K and 1173 K, respectively. The high oxygen level enhanced radical formation, significantly increasing the NO production and shifting N_2O formation to lower temperatures, peaking at 1373 K. At temperatures between 1173 and 1373 K part of the NO was oxidized to NO_2, mainly through $NO + HO_2$ (R17). In both cases, HNCO consumption proceeded more slowly than that of NH_3, with the difference becoming more pronounced at higher O_2 concentrations. This is due to the fact that both components compete for O/H radicals and the NH_3 oxidation reactions are faster than those of HNCO. The kinetic model accurately reproduces the experimental trends across the temperature range.

4.2.1. Effect of CO

The impact of CO on urea oxidation was examined at concentrations of 250 and 1000 ppm as shown in Fig. 6. The presence of CO significantly enhanced the consumption of NH_3 and HNCO, shifting the reaction to lower temperatures; from 1273 K at 0 ppm of CO to 1073 K at 1000 ppm of CO. As the CO concentration increased, the outlet NO level rose accordingly, doubling at 1000 ppm CO compared to the case without CO. The N_2O profile shifted to lower temperatures, peaking at 1473 K, 1373 K, and 1173 K for 0, 250, and 1000 ppm of CO, respectively.

The model predictions for NH_3, HNCO, N_2O, CO and CO_2 are in satisfactory agreement with the measurements. However, NO concentrations are consistently overpredicted by the model under conditions of high CO concentration and elevated temperatures. The discrepancies with the model are investigated in more detail in Section 4.4.

Fig. 7 presents the reaction path diagram for oxidation of urea under the present conditions. Red arrows highlight reactions that are enhanced by the presence of CO. Urea rapidly decomposes into NH_3 and HNCO. Initially, the reaction $HNCO + H_2O = NH_3 + CO_2$ (R2) plays an

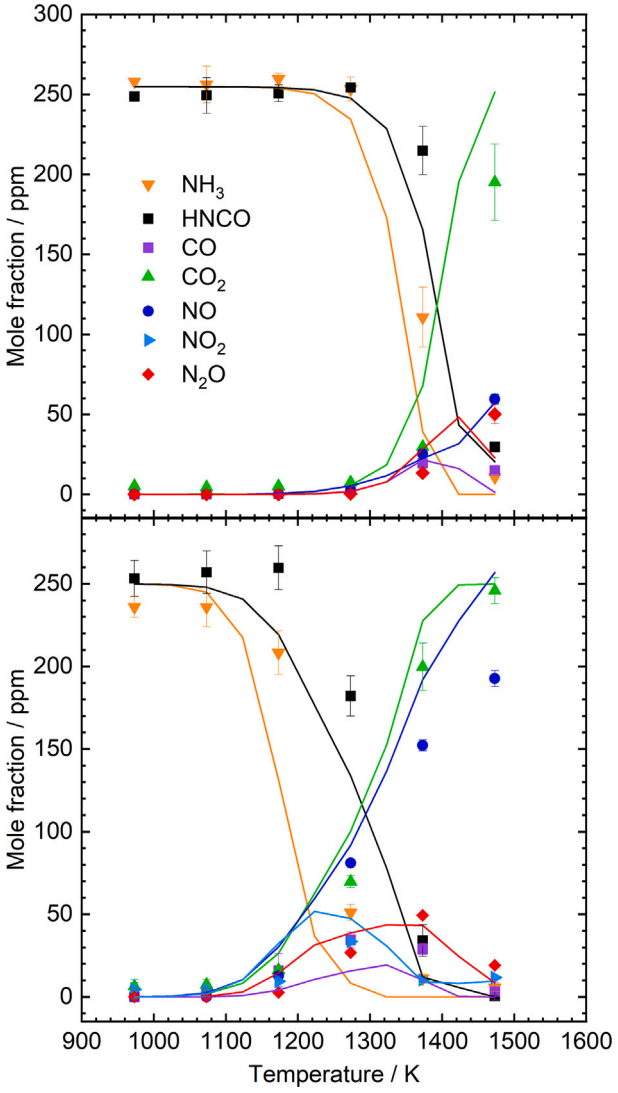

Fig. 5. Urea oxidation as a function of temperature. Symbols represent experimental data, while solid lines denote predictions from the PFR model. Error bars indicate the standard deviation from replicate experiments. *Upper figure*: Inlet mole fractions: $CO(NH_2)_2$ = 255 ppm, O_2 = 5.0 %, H_2O = 3.3 %, balance N_2. *Lower figure*: Inlet mole fractions: $CO(NH_2)_2$ = 250 ppm, O_2 = 97.4 %, H_2O = 2.6 %. P = 1.05 atm. The residence time in the isothermal zone was 101/T[K]s (constant mass flow).

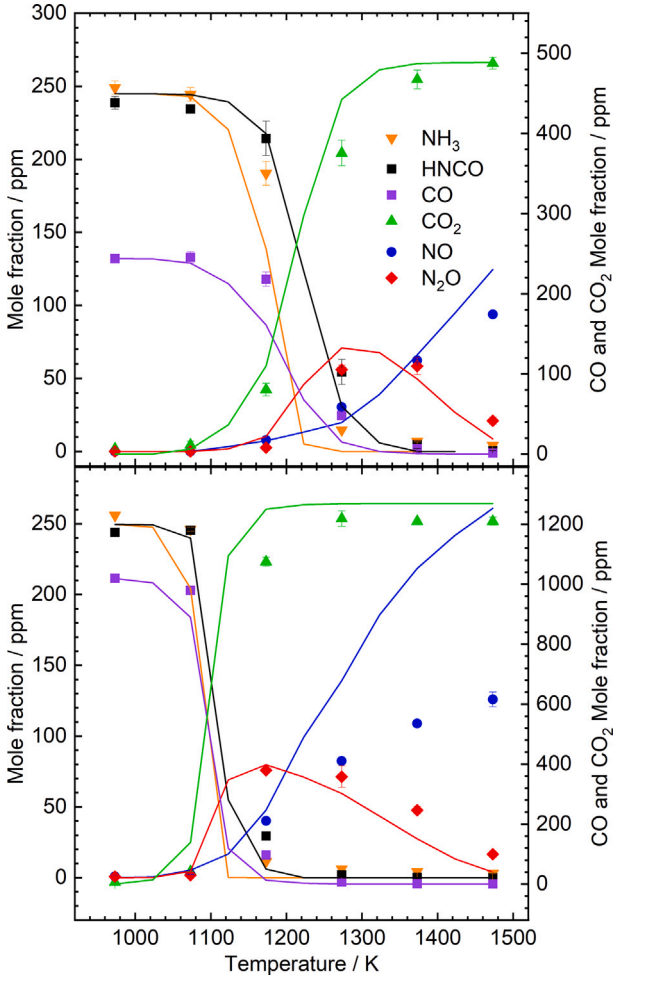

Fig. 6. Effect of CO on the oxidation of urea. Symbols represent experimental data, while solid lines denote predictions from the PFR model. Error bars indicate the standard deviation from replicate experiments. *Upper figure*: Inlet mole fractions: $CO(NH_2)_2$ = 245 ppm, O_2 = 5.0 %, H_2O = 3.4 %, CO = 244 ppm, balance N_2. *Lower figure*: Inlet mole fractions: $CO(NH_2)_2$ = 250 ppm, O_2 = 5.0 %, H_2O = 3.4 %, CO = 1020 ppm, balance N_2. P = 1.05 atm. The residence time in the isothermal zone was 101/T[K]s (constant mass flow).

important role. However, as the reaction progresses, more OH radicals are generated, primarily through the reactions O + H_2O = OH + OH (-R19) and H + O_2 = O + OH (R20). This increase in OH radicals promotes the oxidation of NH_3 and HNCO into NH_2 and NCO radicals. At high temperatures, NH_2 may further react with O_2, OH, or O radicals to form NO via H_2NO (R12), NH (R11), or HNO (R10). Similarly, NCO undergoes oxidation via reactions R5 and R6, producing NO. Alternative minor pathways include NH_2 + NO (R13, R14) and NCO + NO (R7, R8). In the presence of oxygen, CO acts to replenish the radical pool and shifts the NH_3 and HNCO chemistry toward lower temperatures through the chain branching sequence: CO + OH = CO_2 + H (R18), H + O_2 = O + OH (R20), and O + H_2O = OH + OH (-R19). Importantly, CO addition does not change the dominant reaction pathways for NH_3 and HNCO oxidation but accelerates their rates by enhancing radical production.

Fig. 8 shows a sensitivity analysis for NH_3 and HNCO under oxidizing conditions in the absence of CO (at 1373 K) and in the presence of 1000 ppm of CO (at 1073 K). At both temperatures, the sensitivity coefficients are higher for reactions in the amine subset than for HNCO reactions, suggesting that the urea oxidation process is more influenced by NH_3. Small variations in the initial NH_3 conditions have a greater impact on the system's response compared to HNCO. Without CO,chain-branching reactions such as NH_2 + NO = NNH + OH (R14) and NH_2 + O_2 = H_2NO + O (R12) exhibit negative sensitivity coefficients, thereby promoting the NH_3 and HNCO consumption. In contrast, terminating reactions like NH_2 + NO = N_2 + H_2O (R13) and HO_2 + OH = H_2O + O_2 (R22) act to inhibit the reaction progress. In the presence of CO, the competition between H + O_2 = O + OH (R20) and H + O_2 (+M) = HO_2 (+M) (R21) is important for the oxidation rate of NH_3 and HNCO. Both reactions show significant sensitivity coefficients, with (R20) promoting reaction and (R21) slowing down the consumption of both species. In addition, the chain propagating reaction CO + OH = CO_2 + H (R18) shows a significant negative coefficient, thus promoting the reduction of NH_3 and HNCO.

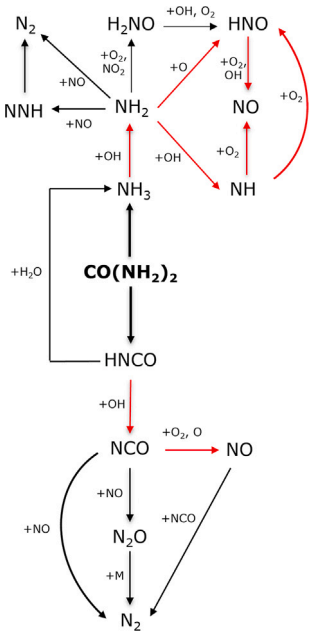

Fig. 7. Reaction path diagram for urea oxidation at 973–1473 K. The red arrows indicate the reactions promoted by the presence of CO. (For interpretation of the references to color in this legend, the reader is referred to the web version of this article.)

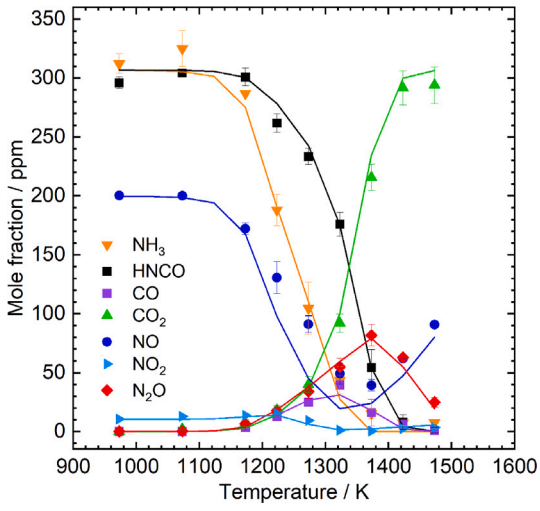

Fig. 9. Comparison of experimental data and modeling predictions for the NO_xOut Process. Symbols represent experimental data, while solid lines denote predictions from the PFR model. Error bars indicate the standard deviation from replicate experiments. Inlet conditions: $CO(NH_2)_2$ = 305 ppm, NO = 200 ppm, NO_2 = 11 ppm, O_2 = 5.0 %, H_2O = 3.6 % and N_2 balance. P = 1.05 atm. The residence time in the isothermal zone was 101/T[K]s (constant mass flow).

4.3. NO_xOut process

The selective non-catalytic reduction of NO using urea was studied at β of 2.9, where β is defined as $\beta = (2 \cdot \text{ppmv}_{\text{UREA}}/\text{ppmv}_{\text{NO+NO}_2})_{\text{FEED}}$. The temperature window for NO removal was between 1123 and 1473 K, with a maximum reduction of 80 % at 1373 K. Between these temperatures, NH_3 and HNCO were oxidized by reacting with OH, producing NH_2 and NCO radicals, which reacted further with NO and led to the observed minimum in NO and maximum in N_2O. Below 1123 K, reaction rates were too slow to enable significant NO reduction, and both NH_3 and HNCO remained largely unconverted. At higher temperatures, i.e, greater than 1373 K, NH_2 and NCO radicals tended to oxidize to form NO rather than reduce it, while N_2O decreased, partly by thermal dissociation. The initial NO_2 concentration originates from some oxidation of NO at low temperatures. Model predictions are in good agreement with experimental data across the investigated temperature range (Fig. 9).

The temperature window where NO is reduced depends on multiple factors, including the flue gas composition, residence time, and mixing. Rota et al. [20] studied the effect of different oxygen concentrations in a jet-stirred reactor, as shown in Fig. 10, and observed a shift of the temperature window towards lower values as the oxygen concentration increased, with a slight decrease in the maximum abatement. Similar shifts in the temperature window with increasing O_2 concentration were also reported by Alzueta et al. [16]. They found

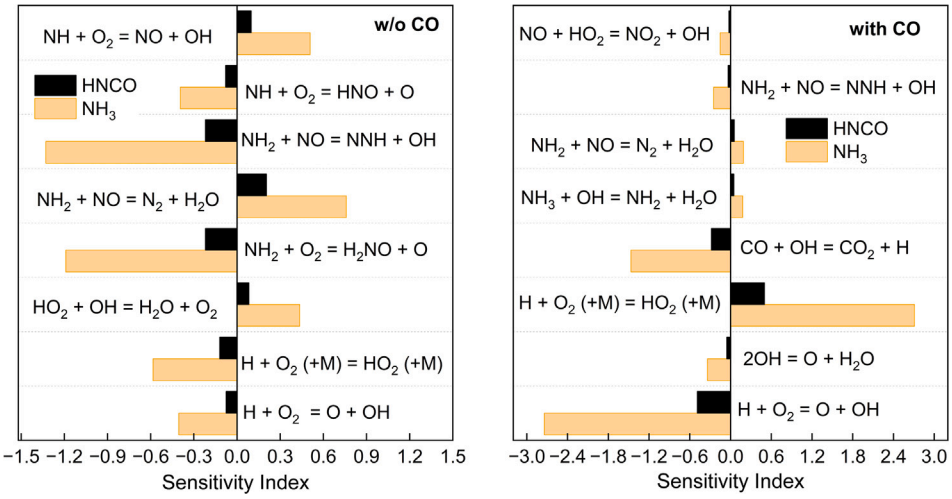

Fig. 8. Sensitivity analysis for HNCO and NH_3 under oxidizing conditions in absence and presence of CO. *Left*: Temperature = 1373 K, $CO(NH_2)_2$ = 256 ppm, O_2 = 5.0 %, H_2O = 3.3 %, balance N_2. *Right*: Temperature = 1073 K, $CO(NH_2)_2$ = 256 ppm, O_2 = 5.0 %, H_2O = 3.3 %, CO = 1000 ppm, balance N_2. P = 1.05 atm.

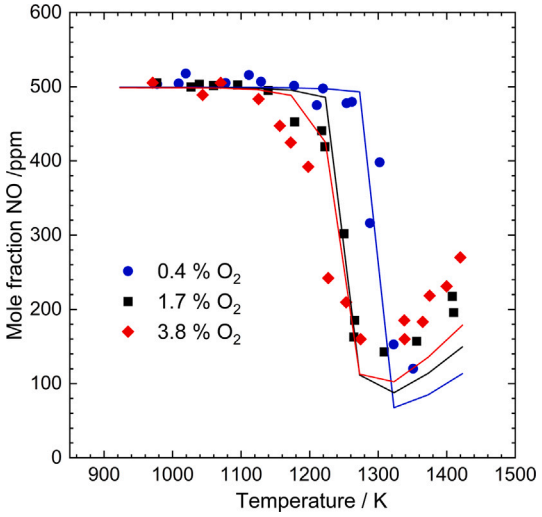

Fig. 10. Comparison of experimental results of Rota et al. [20] for urea SNCR with different oxygen concentration in a jet stirred reactor with modeling predictions. The symbols denote experimental data, while the solid lines denote modeling predicted values. Inlet conditions: $CO(NH_2)_2$ = 600 ppm, NO = 500 ppm, O_2 = 0.4, 1.7, or 3.8 %, H_2O = 19 %, N_2 balance.

that the maximum NO reduction decreased when the oxygen concentration increased from 0.5 % to 1 %, while further increases in O_2 levels had no significant effect on NO abatement. The experimental results from Rota et al. [20] are consistent with model predictions, suggesting a slight shift of the temperature window, while a small increase in maximum NO abatement was observed when lowering the oxygen concentration.

4.3.1. *Effect of CO on NO_xOut process*

The influence of CO on the NO_xOut process is illustrated in Fig. 11. As the CO concentration increased, the temperature window for removal of NO_x (sum of NO and NO_2) shifted to lower temperatures, narrowing the window while maintaining efficiency between 77–80 %. The temperature corresponding to maximum NO_x reduction shifted from 1373 K (without CO) to 1273 K at 250 ppm CO, and further down to 1123 K at 1000 ppm CO. N_2O concentrations increased with rising CO concentration, peaking where the NO_x concentration was at its minimum. The model predictions align well for 0 and 250 ppm of CO, but they overestimate the NO_x concentration at temperatures above 1223 K. A similar overprediction at 1000 ppm CO was previously noted in Fig. 6 and is further analyzed in Section 4.4. A shift to lower temperatures in the NO abatement temperature window due to the presence of CO has been reported by several authors. Lee and Kim [61] examined the CO effect in a pilot-scale stainless steel flow reactor. They observed that, at a CO/urea molar ratio of 1, the temperature at which maximum NO reduction occurred shifted 100 K toward lower values. Similarly, Javed et al. [18], using a laboratory-scale stainless steel flow reactor, found that at a CO/urea molar ratio of 1.5, the temperature for maximum NO reduction decreased by 150 K, from 1373 K to 1223 K. However, results from stainless steel reactors should be interpreted with caution in modeling studies, as steel surfaces may catalyze HNCO reactions, potentially influencing the observations.

To gain further insight into the influence of CO, additional experiments were conducted at 1173 K, analyzing NO, NO_2, and N_2O concentrations as a function of CO level (Fig. 12). This temperature was chosen because, in the absence of CO, little NO removal and N_2O formation occur. The results indicate that at CO concentrations up to 800 ppm, the NCO + NO and NH_2 + NO reactions are promoted

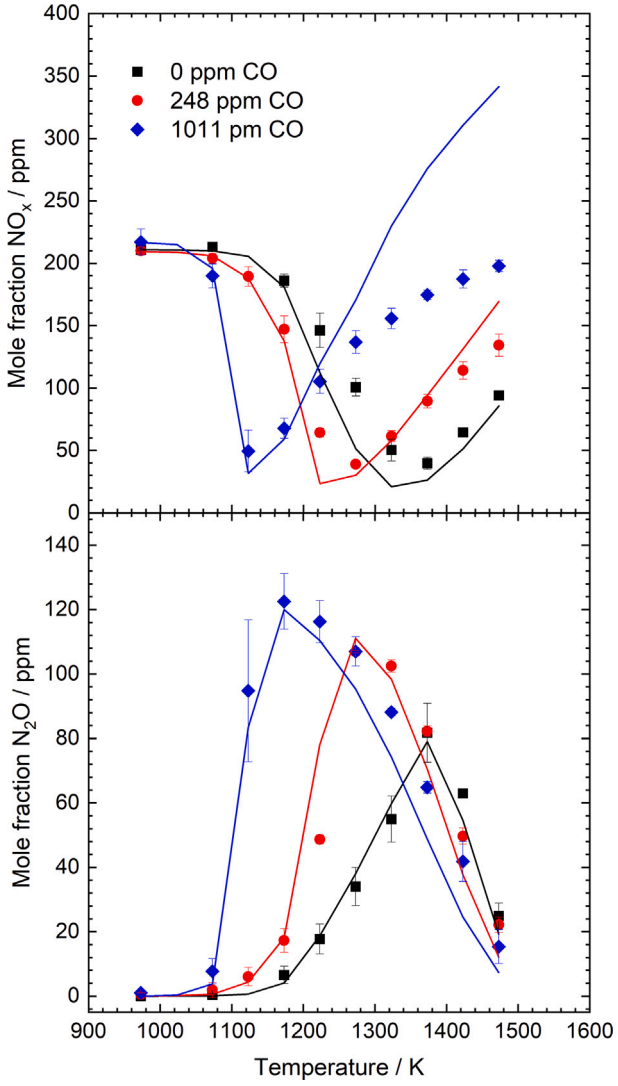

Fig. 11. Effect of CO on the NO_xOut Process. Symbols represent experimental data, while solid lines denote predictions from the PFR model. Error bars indicate the standard deviation from replicate experiments. *0 ppm of CO*: Inlet conditions: $CO(NH_2)_2$ = 305 ppm, NO = 200 ppm, NO_2 = 11 ppm, O_2 = 5.0 %, H_2O = 3.6 % and N_2 balance. *248 ppm of CO*: Inlet conditions: $CO(NH_2)_2$ = 300 ppm, NO = 181 ppm, NO_2 = 28 ppm, CO = 248 ppm, O_2 = 5.0 %, H_2O = 3.2 % and N_2 balance. *1011 ppm of CO*: Inlet conditions: $CO(NH_2)_2$ = 312, NO = 187 ppm, NO_2 = 30 ppm, CO = 1011 ppm, O_2 = 5 %, H_2O = 3.3 % and N_2 balance. P = 1.05 atm. The residence time in the isothermal zone was 101/T[K]s (constant mass flow).

and the NO abatement temperature window is shifted to lower temperatures. However, at higher CO levels, NO concentrations begin to rise again. This could be attributed to the excess availability of O/OH radicals, which promote the oxidation pathways of NCO and NH_2 to NO. The model predictions satisfactorily agree with the experimental results.

Fig. 13 presents the reaction path diagram for the NO_xOut process. In the presence of NO, NH_3 and HNCO start to be consumed at lower temperatures compared to the urea oxidation case (1073 K vs. 1273 K, respectively). This behavior is mainly due to propagating and branching reactions with NO. These include NH_2 + NO = NNH + OH (R14) and NO + HO_2 = NO_2 + OH (R17), which lead to the generation of OH radicals.

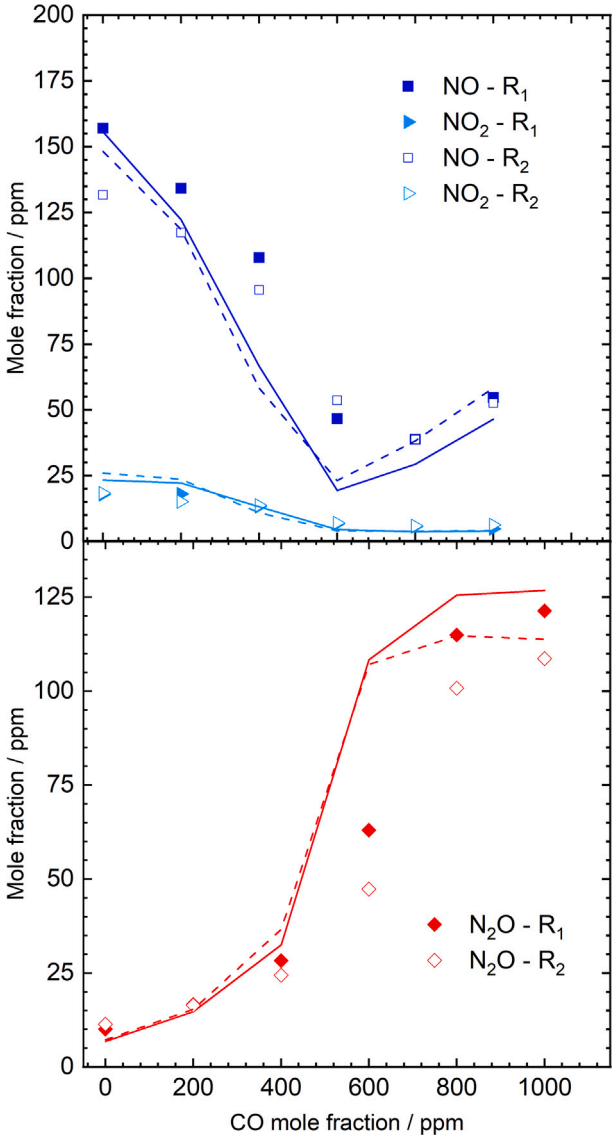

Fig. 12. Effect of CO concentration at 1173 K on NO reduction. Symbols represent experimental data: filled symbols correspond to repetition 1 (R_1) and empty symbols to repetition 2 (R_2). The lines indicate the predicted values from the PFR model: the solid line for R_1 and the dashed line for R_2. *Average inlet conditions* R_1: $CO(NH_2)_2$ = 341 ppm, NO = 194 ppm, NO_2 = 22 ppm, O_2 = 5 %, H_2O = 3.2 %, and N_2 as balance gas. *Average inlet conditions* R_2: $CO(NH_2)_2$ = 299 ppm, NO = 184 ppm, NO_2 = 25 ppm, O_2 = 5 %, H_2O = 3.1 %, and N_2 as balance gas. P = 1.05 atm. The residence time in the isothermal zone was 101/T[K] (constant mass flow).

Above 1073 K, NO is primarily consumed through the NH_2 + NO (R13, R14) and NCO + NO (R7, R8) reactions. To a lesser extent, NH_2 may also react with NO_2, producing NO instead of reducing it via H_2NO → HNO → NO. However, between 1073 K and 1373 K, the reduction of NO remains the dominant process. As NO abatement begins, the NH_3 consumption rate is faster than that of HNCO, leading to the generation of more NH_2 radicals. This favors the NH_2 + NO reaction over the NCO + NO reaction. As the temperature increases further, the rate of HNCO consumption rises, and the NCO + NO = N_2O + CO (R7) and NCO + NO = N_2 + CO_2 (R8) reactions become prominent, with R7 constituting the main N_2O formation pathway. Above 1373 K, N_2O dissociates to generate atomic O, which leads to the formation of OH (-R19). Under these conditions, oxidation pathways (R5, R6, R10, R11, R12) compete with reduction pathways (R7, R8, R13, R14). As a result, NO levels increase while N_2O concentration decreases.

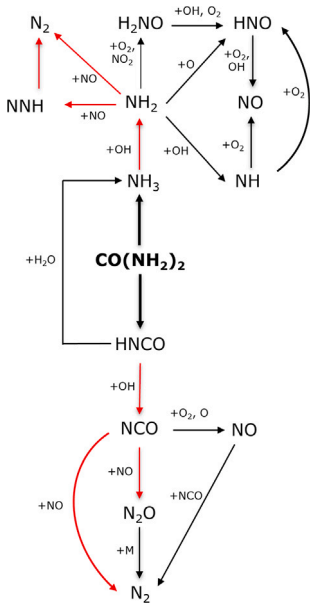

Fig. 13. Reaction path diagram for NO_xOut process at 973–1473 K. The red arrows indicate the reactions promoted by presence of NO. (For interpretation of the references to color in this legend, the reader is referred to the web version of this article.)

Fig. 14 presents a sensitivity analysis for NO and N_2O in the NO_xOut process, both in the absence of CO and in the presence of 1000 ppm of CO at 1273 K. In the NO_xOut process, NH_2 + NO reactions exhibit the largest sensitivity coefficients for both NO and N_2O, due to the competition between a branching (R14) and a terminating (R13) product channel. R14 shows a strong negative sensitivity coefficient for NO and a strong positive one for N_2O, as it generates OH radicals that enhance NO consumption and indirectly promote N_2O formation. On the other hand, R13 is a chain-terminating reaction with a positive coefficient for NO, inhibiting its consumption, and consequently a negative coefficient for N_2O. In the presence of CO, the sensitivity coefficient for NCO + O = NO + CO (R5) becomes significant, promoting NO formation, while inhibiting formation of N_2O. In addition, NCO + NO = N_2O + CO (R7) shows a positive coefficient for N_2O, promoting its direct formation.

4.4. Evaluation of the plug-flow approximation

At high CO concentrations and elevated temperatures, significant discrepancies emerge between the measured NO concentrations and predictions from the plug-flow reactor (PFR) model, as observed in Fig. 6 (*Lower figure*) and Fig. 11 (*at 1011 ppm CO*). Fig. 15 presents the axial concentration profiles of CO and NO at 1473 K (Fig. 11, *1011 ppm CO*), where the model overpredicts NO by nearly a factor of two. The reaction takes place very rapidly within the preheating zone, where steep thermal and concentration gradients are present. Under these conditions, the plug-flow approximation breaks down due to the presence of radial gradients and fast reaction rates.

Fig. 16 illustrates the radial and axial gradients based on 2D simulations. The PFR model neglects radial temperature gradients and assumes a uniform temperature across the radial direction, which, under steep preheating, can lead to an overestimation of the degree of reaction and an artificial overprediction of NO formation.

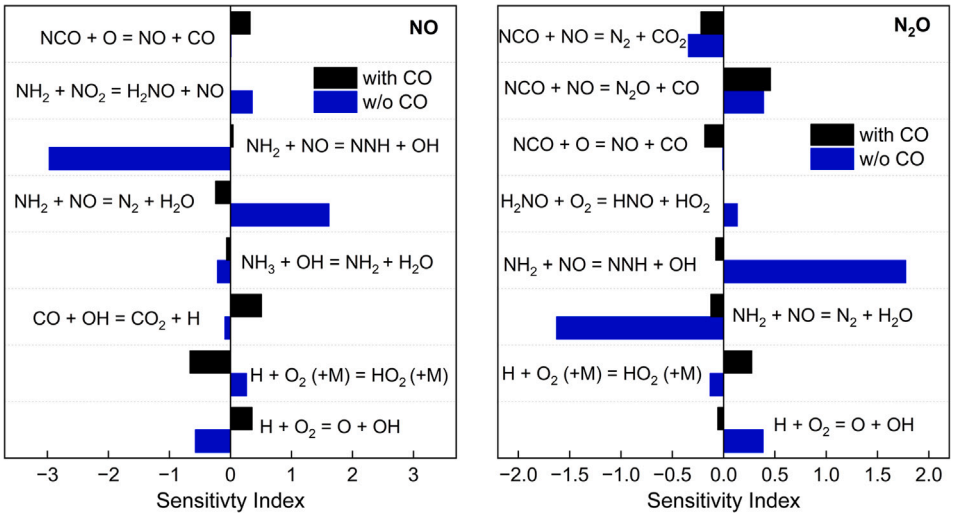

Fig. 14. Sensitivity analysis for NO (left) and N_2O (right) for the NO_xOut process in absence and presence of CO. Inlet conditions: Temperature = 1273 K, $CO(NH_2)_2$ = 305 ppm, O_2 = 5.0 %, H_2O = 3.6 %, NO = 200 ppm, NO_2 = 11.6 ppm, CO = 0 or 1000 ppm, balance N_2. P = 1.05 atm.

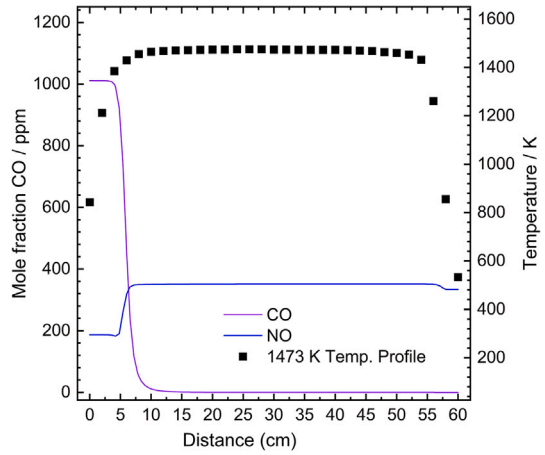

Fig. 15. Evolution of the mole fractions and temperature in the reactor at 1473 K. Inlet conditions: 312 of $CO(NH_2)_2$, 187 ppm of NO, 30 ppm NO_2, 1011 ppm of CO, 5.0 % of O_2, 3.3 % of H_2O and N_2 balance. P = 1.05 atm. The residence time in the isothermal zone was 101/T[K]s (constant mass flow).

Fig. 17 presents a comparison of NO measurements with different reactor models. Fig. 17(*left*) compares the PFR with a cylindrical shear flow reactor (CSFR) and a full two-dimensional axisymmetric reactor including back diffusion (2D). The CSFR incorporates a boundary-layer approximation, that accounts for radial diffusion and dispersion of species, mass, and energy. However, convection is assumed to dominate in the axial direction, and the axial diffusion is neglected. In the 2D simulations, diffusion was accounted for in both the radial and axial directions. Both the CSFR and the 2D model show good agreement with the experimental results, suggesting that radial thermal dispersion is crucial especially in the preheating zone, where reaction rate sensitivity to temperature is high. Additional comparisons for NH_3, HNCO, NO_2, and N_2O are provided in the Supplementary Material, where minor deviations across the models are observed. Comparisons of the reactor models in the absence of CO are included in the Supplementary Material, in which the chemistry proceeds more slowly and predominantly within the isothermal zones. Under these conditions, radial gradients are less pronounced, and the plug-flow approximation remains valid.

To further investigate the origin of the discrepancies between the plug-flow reactor (PFR) and the two-dimensional axisymmetric reactor model, a series of additional one-dimensional simulations were conducted. The results of these comparisons are presented in Fig. 17 (*right*). These simulations aimed to isolate the effects of axial diffusion, axial conduction, and the coupling between radial transport and axial dispersion (Taylor-Aris effect). Four different 1D models were considered:

- A fully laminar 1D model, accounting for axial diffusion and conduction.
- A 1D model including Taylor-Aris corrections for both mass and heat transport.
- A 1D model with Taylor-Aris correction for heat transport only.
- A 1D model with Taylor-Aris correction for mass transport only.

The results show that the fully laminar 1D model, the 1D-TA (Mass) and the PFR model produced nearly identical results across all temperatures, indicating that axial diffusion and conduction have a negligible impact under the investigated conditions. Enhanced mass dispersion alone does not impact results significantly, likely because species gradients are not steep enough for dispersion to matter without heat feedback. The inclusion of Taylor-Aris corrections for heat transport, either alone or combined with mass transport, led to results that were closer to those of the 2D model and the CSFR model, supporting the idea that the main discrepancy is due to effective radial thermal transport, which is mimicked quite well by the TA correction and naturally captured in CSFR and 2D. Overall, it confirms that while the PFR model provides reliable predictions in most conditions, radial effects and heat transport become critical in scenarios where fast chemistry occurs under strong thermal gradients.

These results demonstrate that while plug-flow assumptions may suffice under moderate conditions, systems involving fast reactions in thermally non-uniform regions require multidimensional modeling approaches, such as CSFR or 2D simulations, to accurately capture the interplay between heat transport and chemical kinetics.

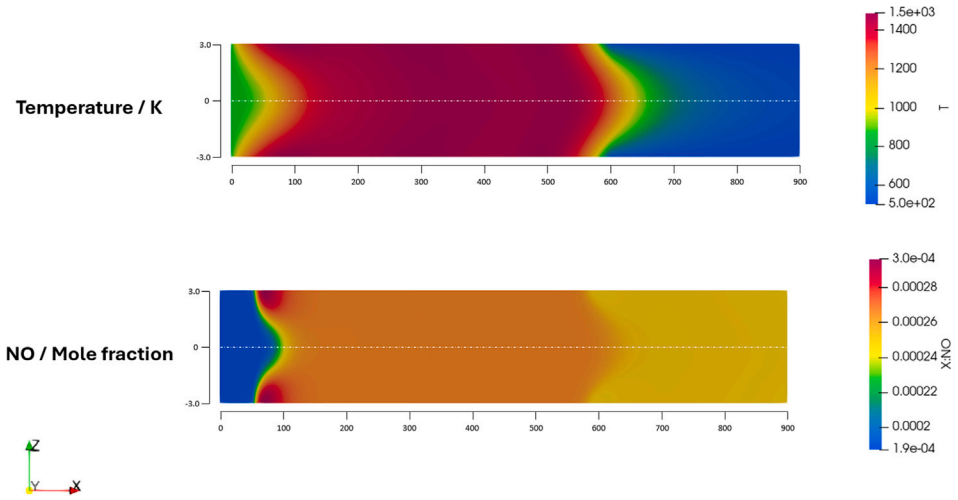

Fig. 16. Contour map at 1473 K for the initial conditions of Fig. 11 (*at 1011 ppm CO*), using a full two-dimensional axisymmetric reactor model.

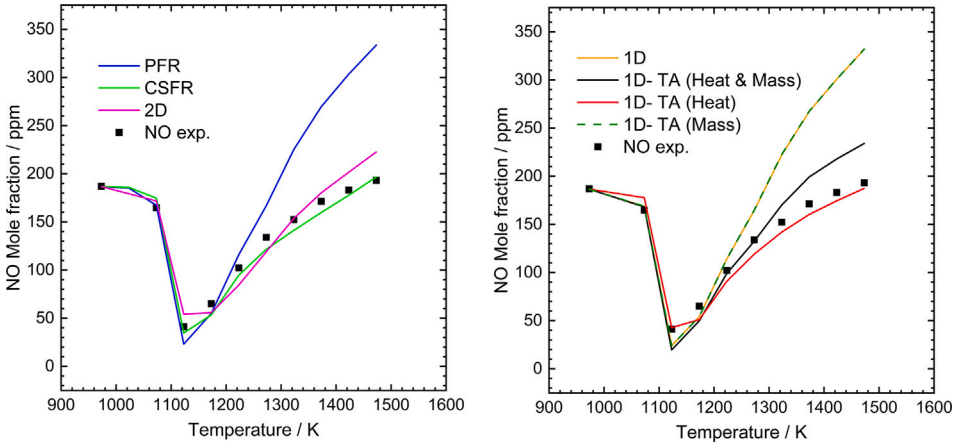

Fig. 17. Comparison of NO measurements with different reactor models. *Left*: PFR model, CSFR, and 2D model. *Right*: 1D and 1D-TA models (Heat, Mass, and Heat & Mass). Inlet mole fractions: $CO(NH_2)_2$ = 312 ppm, NO = 187 ppm, NO_2 = 30 ppm, O_2 = 5.0 %, H_2O = 3.3 %, CO = 1011 ppm, balance N_2. P = 1.05 atm. The residence time in the isothermal zone was 101/T [K] s (constant mass flow).

5. Conclusions

In the present work, urea decomposition and oxidation at high temperatures, as well as the NO_xOut process, have been studied both experimentally and through chemical kinetic modeling. The following conclusions can be made:

- Thermal urea decomposition and oxidation experiments show good agreement with model predictions and are consistent with the rate constant for dissociation calculated by Honorien et al. [32]. The results indicate that even for urea-water droplets, decomposition occurs in the gas-phase.
- CO addition has a similar impact on both urea oxidation and the NO_xOut process, shifting the chemistry towards lower temperatures. In the NO_xOut process, the maximum NO removal shifted by up to 200 K while maintaining the efficiency. Model predictions align well with experimental results and with data from the literature.
- At high temperatures and CO concentrations, the plug-flow approximation becomes inadequate due to radial temperature gradients in the preheating zone. Under these conditions, CSFR and 2D models provide more reliable predictions.
- This study highlights the need for multidimensional modeling to accurately capture the interplay between heat and mass transport in fast-reacting zones, particularly under high CO loading.

CRediT authorship contribution statement

Claudia Pastor-Morell: Writing – original draft, Methodology, Investigation, Conceptualization. **Hamid Hashemi:** Writing – review & editing, Supervision. **Hao Wu:** Writing – review & editing, Supervision. **Peter Glarborg:** Writing – review & editing, Supervision. **Alberto Cuoci:** Writing – review & editing, Investigation.

Declaration of competing interest

The authors declare that they have no known competing financial interests or personal relationships that could have appeared to influence the work reported in this paper.

Acknowledgments

The project has received financial support from the Sino-Danish Center for Education and Research, Denmark and from the Technical University of Denmark.

Appendix A. Supplementary data

Supplementary data for this article can be found online at doi:10.1016/j.fuel.2026.138537.

Data availability

Data will be made available on request.

References

[1] European Commission. Commission implementing decision (EU) 2019/2010 establishing the best available techniques (BAT) conclusions, under directive 2010/75/EU of the european parliament and of the council, for waste incineration. Official J European Union 2019:55–91.

[2] Tayyeb Javed M, Irfan N, Gibbs BM. Control of combustion-generated nitrogen oxides by selective non-catalytic reduction. J Environ Manage 2007;83:251–89.

[3] Liang L, Hui S, Pan S, Shang T, Liu C, Wang D. Influence of mixing, oxygen and residence time on the SNCR process. Fuel 2014;120:38–45.

[4] Mladenović M, Paprika M, Marinković A. Denitrification techniques for biomass combustion. Renew Sustain Energy Rev 2018;82:3350–64.

[5] Gholami F, Tomas M, Gholami Z, Vakili M. Technologies for the nitrogen oxides reduction from flue gas: a review. Sci Total Environ 2020;714:136712.

[6] Lyon RK, Hardy JE. Discovery and development of the thermal DeNO$_x$ process. Ind Eng Chem Fundam 1986;25:19–24.

[7] Miller JA, Bowman CT. Mechanism and modeling of nitrogen Chemistry in combustion. Prog Energy Combust Sci 1989;15:287–338.

[8] Miller JA, Glarborg P. Modelling the formation of N_2O and NO_2 in the thermal de-NO$_x$ process. In: Springer ser. Chem. Phys, vol. 61. Springer Berlin Heidelberg; 1996. p. 318–33.

[9] Muzio LJ, Arand JK, Teixeira DP. Gas phase decomposition of nitric oxide in combustion products. Symp Int Combust 1977;16:199–208.

[10] Glarborg P, Miller JA, Ruscic B, Klippenstein SJ. Modeling nitrogen Chemistry in combustion. Prog Energy Combust Sci 2018;67:31–68.

[11] Sahu J, Hussain S, Meikap B. Studies on the hydrolysis of urea for production of ammonia and modeling for flow characterization in presence of stirring in a batch reactor using computational fluid dynamics. Korean J Chem Eng 2011;28:1380–5.

[12] Wang D, Hui S, Liu C, Zhuang H. Effect of oxygen and additives on thermal decomposition of aqueous urea solution. Fuel 2016;180:34–40.

[13] Jepsen MS. NO$_x$ reduction in grate-fired waste-to-energy plants, PhD thesis. DTU Chemical Engineering, Technical University of Denmark; 2018.

[14] Lodder P, Lefers JB. Effect of natural gas, C_2H_6 and CO on the homogeneous gas phase reduction of NO$_x$ by NH_3. Chem Eng J 1985;30:161–7.

[15] Brouwer J, Heap MP, Pershing DW, Smith PJ. A model for prediction of selective noncatalytic reduction of nitrogen oxides by ammonia, urea, and cyanuric acid with mixing limitations in the presence of CO. Symp Int Combust 1996;26:2117–24.

[16] Alzueta MU, Bilbao R, Millera Á Oliva AM, Ibáñez JC. Interactions between nitric oxide and urea under flow reactor conditions. Energy Fuels 1998;12:1001–7.

[17] Bae SW, Roh SA, Kim SD. NO removal by reducing agents and additives in the selective non-catalytic reduction (SNCR) process. Chemosphere 2006;65:170–5.

[18] Javed MT, Nimmo W, Gibbs BM. Experimental and modeling study of the effect of CO and H_2 on the urea DeNO$_x$ process in a 150kw laboratory reactor. Chemosphere 2008;70:1059–67.

[19] Lee S, Park K, Park JW, Kim B-H. Characteristics of reducing NO using urea and alkaline additives. Combust Flame 2005;141:200–3.

[20] Rota R, Antos D, Zanoelo EF, Morbidelli M. Experimental and modeling analysis of the NO$_x$OUT process. Chem Eng Sci 2002;57:27–38.

[21] Rota R, Zanoelo EF. Influence of oxygenated additives on the NO$_x$OUT process efficiency. Fuel 2003;82:765–70.

[22] Alzueta MU, Bilbao R, Millera Á Oliva M, Ibáñez JC. Impact of new findings concerning urea thermal decomposition on the modeling of the urea-SNCR process. Energy Fuels 2000;14:509–10.

[23] Abu-Ramadan E, Saha K, Li X. Modeling the depleting mechanism of urea water solution droplet for automotive selective catalytic reduction systems. AIChE J 2011;57:3210–25.

[24] Daïf A, Bouaziz M, Chesneau X, Cherif AA. Comparison of multicomponent fuel droplet vaporization experiments in forced convection with the sirignano model. Exp Therm Fluid Sci 1998;18:282–90.

[25] Wang TJ, Baek SW, Lee SY, Kang DH, Yeo GK. Experimental investigation on evaporation of urea-water-solution droplet for SCR applications. AIChE J 2010;55:3267–76.

[26] Stein M, Bykov VV, Maas U. The effect of evaporation models on urea decomposition from urea-water-solution droplets in SCR conditions. Emiss Control Sci Technol 2017;3:263–74.

[27] Jian J, Hashemi H, Wu H, Glarborg P, Jasper AW, Klippenstein SJ. An experimental, theoretical, and kinetic modeling study of post-flame oxidation of ammonia. Combust Flame 2024;261:113325.

[28] Morell CP, Juhl CK, Chanpirak A, Hashemi H, Wu H, Glarborg P. Re-examination of the HNCO oxidation Chemistry. Fuel 2025;385:134090.

[29] Manual TSI instruction. Model 3075/3076 constant output atomizer. www.manualslib.com/manual/3044972/Tsi-Instruments. 2009.

[30] Glarborg P. The $NH_3/NO_2/O_2$ system: constraining key steps in ammonia ignition and N_2O formation. Combust Flame 2023;257:112311.

[31] Glarborg P, Allingham JS, Skov AB, Hashemi H, Marshall P. Re-examination of the N_2O + O reaction. J Phys Chem A 2023;127:6521–31.

[32] Honorien J, Fournet R, Glaude P-A, Sirjean B. Theoretical study of the gas-phase thermal decomposition of urea. Proc Combust Inst 2021;38:355–64.

[33] Mertens JD, Chang AY, Hanson RK, Bowman CT. Reaction-kinetics of NH in the shock-tube pyrolysis of HNCO. Int J Chem Kinet 1989;21:1049–67.

[34] Wooldridge ST, Hanson RK, Bowman CT. A shock tube study of CO + OH → CO_2 + h and HNCO + OH → products via simultaneous laser absorption measurements of OH and CO_2. Int J Chem Kinet 1995;28:361–72.

[35] Gao Y, MacDonald G. Determination of the rate constant for the NCO + O reaction at 292 k. J Phys Chem A 2003;107:4625–35.

[36] Miller JA, Bowman CT. Kinetic modeling of the reduction of nitric oxide in combustion products by isocyanic acid. Int J Chem Kinet 1991;23:289–313.

[37] Zhu RS, Lin MC. The NCO + NO reaction revisited: AB inito MO/VRRKM calculations for total rate constant and product branching ratios. J Phys Chem A 2000;104:10807–11.

[38] Salimian S, Hanson RK, Kruger CH. High temperature study of the reactions of O and OH with NH_3. Int J Chem Kinet 1984;16:725–39.

[39] Klippenstein SJ, Mulvihill CR, Glarborg P. Theoretical kinetics predictions for reactions on the NH_2O potential energy surface. J Phys Chem A 2023;127:8650–62.

[40] Klippenstein SJ, Harding LB, Ruscic B, Sivaramakrishnan R, Srinivasan NK, Su M-C, Michael JV. Thermal decomposition of NH_2OH and subsequent reactions: AB initiotransition state theory and reflected shock tube experiments. J Phys Chem A 2009;113:10241–59.

[41] Klippenstein SJ, Harding LB, Glarborg P, Miller JA. The role of NNH in NO formation and control. Combust Flame 2011;158:774–89.

[42] Song S, Hanson RK, Bowman CT, Golden DM. Shock tube determination of the overall rate of NH_2 + NO → products in the thermal de-NO$_x$ temperature window. Int J Chem Kinet 2001;33:715–21.

[43] Römming H-J, Wagner HG. A kinetic study of the reactions of NH($^3\Sigma^-$) with O_2 and NO in the temperature range from 1200 to 2200 k. Symp Int Combust 1996;26:559–66.

[44] Baulch DL, Bowman CT, Cobos CJ, Cox RA, Just T, Kerr JA, Pilling MJ, Stocker D, Troe J, Tsang W, Walker RW, Warnatz J. Evaluated kinetic data for combustion modeling: supplement II. J Phys Chem Ref Data 2005;34:757–1397.

[45] Senosiain JP, Klippenstein SJ, Miller JA. A complete statistical analysis of the reaction between OH and CO. Proc Combust Inst 2005;30:945–53.

[46] Hong Z, Davidson DF, Barbour EA, Hanson RK. A new shock tube study of the H + O_2 → OH + O reaction rate using tunable diode laser absorption of H_2O near 2.5 μm. Proc Combust Inst 2011;33:309–16.

[47] Lei L, Burke MP. Mixture rules and falloff as major uncertainties in experimentally derived rate parameters for H + O_2 (+M) ↔ HO_2 (+M). Combust Flame 2020;213:467–74.

[48] Burke MP, Klippenstein SJ, Harding LB. A quantitative explanation for the apparent anomalous temperature dependence of OH + HO_2 = H_2O + O_2 through multiscale modeling. Proc Combust Inst 2013;34:547–55.

[49] Caton JA, Siebers DL. Comparison of nitric oxide removal by cyanuric acid and by ammonia. Combust Sci Technol 1989;65:277–93.

[50] Koebel M, Elsener M. Entstickung von abgasen nach DEM SNCR-verfahren: ammoniak oder harnstoff als reduktionsmittel? Chem Ing Tech 1992;64:934–7.

[51] Itaya Y. NO reduction behavior by urea solution injection in the tubular reactor. Environ Comb Tech 2001;2:345–59.

[52] Koebel M, Strutz EO. Thermal and hydrolytic decomposition of urea for automotive selective catalytic reduction systems: thermochemical and practical aspects. Ind Eng Chem Res 2003;42:2093–100.

[53] Aoki H, Fujiwara T, Morozumi Y, Miura T. Measurement of urea thermal decomposition reaction rate for NO selective non-catalytic reduction. In: Fifth international conference on technologies and combustion for a clean environment, vol. 1, 1999, p. 115–8.

[54] Yim S-D, Kim SJ, Baik JH, Nam IS, Mok YS, Lee JH, Cho BK, Oh S. Decomposition of urea into NH_3 for the SCR process. Ind Eng Chem Res 2004;43:4856–63.

[55] Jødal M, Nielsen C, Hulgaard T, Dam-Johansen K. Pilot-scale experiments with ammonia and urea as reductants in selective non-catalytic reduction of nitric oxide. Symp Int Combust 1990;23:237–43.

[56] Bilbao R, Oliva M, Ibanez JC, Zapater A, Millera A, Alzueta MU. The use of urea as selective non-catalytic reduction agent to reduce NO$_x$ emissions. In: Ziegler A, van Heek KH, Klein J, Wanzl W, editors. 9. International Conference on Coal Science (ICCS '97). Vol. 3. Proceedings. 690 p. 1997.

[57] Ansys, Inc. Ansys chemkin-PRO 2022 r2. 2022, Ansys, Inc., Canonsburg, PA, chemical kinetics simulation software.

[58] Cuoci A, Frassoldati A, Faravelli T, Ranzi E. Numerical modeling of laminar flames with detailed kinetics based on the operator-splitting method. Energy Fuels 2013;27:7730–53.

[59] Cuoci A, Frassoldati A, Faravelli T, Ranzi E. A computational tool for the detailed kinetic modeling of laminar flames: application to C_2H_4/CH_4 coflow flames. Combust Flame 2013;160:870–86.

[60] Chen Z-C, Yang W-J, Zhou J-H, Lv H-K, Liu J-Z, Cen K-F. HNCO hydrolysis performance in urea-water solution thermohydrolysis process with and without catalysts. J Zhejiang Univ Sci A 2010;11:849–56.

[61] Lee JB, Kim SD. Kinetics of NO$_x$ reduction by urea solution in a pilot scale reactor. J Chem Eng Jpn 1996;29:620–6.